HHS Public Access

Author manuscript

J Orthop Res. Author manuscript; available in PMC 2019 June 01.

Published in final edited form as:

J Orthop Res. 2018 June ; 36(6): 1614–1623. doi:10.1002/jor.23831.

Obesity/type 2 diabetes increases inflammation, periosteal reactive bone formation and osteolysis during *Staphylococcus aureus* implant-associated bone infection

Christopher W Farnsworth[1,2], **Eric M Schott**[1,2], **Abigail Benvie**[1,2], **Jacob Zukoski**[1,2], **Stephen L Kates**[3], **Edward M Schwarz**[2], **Steven R Gill**[4], **Michael J Zuscik**[2], and **Robert A Mooney**[1,2]

[1]Department of Pathology and Laboratory Medicine, University of Rochester, Rochester New York, USA

[2]Center for Musculoskeletal Research, University of Rochester, Rochester New York, USA

[3]Department of Orthopaedic Surgery, Virginia Commonwealth University, Richmond Virginia, USA

[4]Department of Microbiology and Immunology, University of Rochester, Rochester New York, USA

Abstract

Obese and type 2 diabetic (T2D) patients have a 5-fold increased rate of infection following placement of an indwelling orthopaedic device. Though implant infections are associated with inflammation, periosteal reactive bone formation and osteolysis, the effect of obesity/T2D on these complicating factors has not been studied. To address this question, C57BL/6J mice were fed a high fat diet (60% Kcal from fat) to induce obesity/T2D, or a control diet (10% Kcal from fat) for three months, and challenged with a transtibial pin coated with a bioluminescent USA300 strain of *S. aureus*. In the resulting infected bone, obesity/T2D was associated with increased *S. aureus* proliferation and colony forming units. RNA sequencing of the infected tibiae on days 7 and 14 revealed an increase in 635 genes in obese/T2D mice relative to controls. Pathways associated with ossification, angiogenesis, and immunity were enriched. MicroCT and histology on days 21 and 35 demonstrated significant increased periosteal reactive bone formation in infected obese/T2D mice versus infected controls ($p<0.05$). The enhanced periosteal bone formation was associated with increased osteoblastic activity and robust endochondral ossification, with persistant cartilage on day 21 that was only observed in infected obesity/T2D. Osteolysis and osteoclast numbers in obesity/T2D were also significantly increased versus infected controls ($p<0.05$). Consistent with an up-regulated immune transcriptome, macrophages were more abundant within both the periosteum and the new reactive bone of obese/T2D mice. In conclusion, we find that implant-associated *S. aureus* osteomyelitis in obesity/T2D is associated with increased inflammation, reactive bone formation and osteolysis.

Address correspondence to: Robert A. Mooney, Ph.D., Dept. of Pathology and Laboratory Medicine, Box 626, 601 Elmwood Ave., Rochester, NY 14642, 585-275-7811; Fax 585-756-4468. robert_mooney@urmc.rochester.edu.

Author contributions: All authors contributed to the study design, acquisition of data and data analysis. CWK, SLK, EMS, SRG, MJZ, RAM were responsible for drafting and editing the manuscript. All authors read and approved the submitted version.

Keywords

osteomyelitis; obesity; diabetes; *Staphylococcus aureus*; osteolysis; osteoblast

INTRODUCTION

Primary total hip and knee arthroplasties are common procedures, with over 800,000 occurring in the United States annually [1; 2]. While rare, infection of an indwelling device is catastrophic to patients, causing significant morbidity, extended hospital stays, and on some occasions mortality [1; 3]. The costs associated with infection are substantial, averaging $25,000–32,000 per patient [4]. Further complicating this issue, *Staphylococcus aureus* is the infectious agent in approximately 60% of these cases, and over half of the cases are methicillin resistant [1]. *S. aureus* has multiple mechanisms to promote immune evasion, including biofilm formation [5], and the ability to persist in necrotic bone [3; 6]. Thus, reinfection after surgical intervention occurs in 10–30% of cases [7]. While infection of indwelling orthopaedic devices is limited to 1–3% of joint surgeries [2], obese and diabetic patients have a 5-fold increase in infection risk [8–10]. The cause of this increased risk is likely multifactorial, including impairments in innate [11; 12] and adaptive immunity [13; 14]. Moreover, we have recently demonstrated that *S. aureus* adapts to the obese/T2D host by altering gene expression leading to increased virulence and persistence of orthopaedic infections in this population [15]. Despite this, much needs to be determined concerning *S. aureus* orthopaedic infection in obesity/T2D, particularly the effects on bone parameters.

In the course of an implant-associated bone infection, considerable trabecular and cortical bone may become necrotic due to colonization of the osteocytic-canalicular network [16], or resorbed during sequestrum formation [3]. The osteolysis can lead to implant loosening, impaired osseointegration, and pain. Furthermore, in many cases there will be a distinct periosteal reaction, associated with the formation of new bone on the periosteal bone surface, frequently away from the site of infection, often disorganized, and of poor quality [3; 17]. Despite a recognition of the pathologic changes in orthopaedic infection, the molecular mechanisms that drive these processes have not been well studied.

Recently, several *S. aureus* virulence factors have been demonstrated to be pathologic to bone in orthopaedic infection [17]. Aureolysin, a *S. aureus* virulence factor regulated by the locus sae, was found to be critical for pathologic bone destruction in osteomyelitis [18]. Similarly, the phenol soluble modulin sarA was recently shown to modulate bone loss *in vivo* and osteoblast cell death *in vitro* [19]. It is also generally accepted that invading leukocytes and loss of vasculature contribute to bone necrosis [3]. To date, the effect of obesity/T2D on bone structure following orthopaedic *S. aureus* infection has not been studied. In the absence of infection, we have shown that mice fed a high fat-diet have diminished trabecular bone volume because of increased osteoclastogenesis [20]. We have also shown that obese/T2D mice have impaired fracture healing [21]. A contributing factor in these skeletal effects may be the well documented increased systemic inflammation in obesity/T2D [22; 23]. Here we build on our previous work in a mouse model of obesity/T2D and orthopaedic infection to test the hypothesis that the altered host environment of obesity/

T2D, coupled with increased *S. aureus* virulence in this host, drives more severe pathologic bone changes, particularly more severe osteolysis and reactive bone formation.

MATERIALS AND METHODS

Animals

All handling of mice and associated experimental procedures were reviewed and approved by the University Committee on Animal Resources at the University of Rochester Medical Center. Male C57BL/6J mice purchased from Jackson Laboratories (Bar Harbor, ME) were housed five per cage in one-way housing on a 12-hour light/dark cycle at the University of Rochester. To model obesity and T2D, mice were placed on a high fat (60% kcal, D12492) or low-fat (10% kcal D12450J) diet for three months beginning at five weeks of age (Open Source Diets, Research Diets Inc., New Brunswick, NJ). Prior to infection, fasting blood glucose levels were measured using One Touch glucose meters (Lifescan Inc., Milpitas, CA) after an overnight fast. Glucose tolerance testing was also performed on mice fasted overnight. Lean and HF-fed mice had an average fasting blood glucose of 120mg/dL and 190mg/dL, respectively. All metabolic changes due to HF feeding were comparable to those that we have reported previously [13; 15; 20; 24].

Orthopaedic implant surgery and infection

An orthopaedic implant, coated with *S. aureus*, was placed as described previously [13]. In brief, a flat stainless steel surgical wire was cut to .02 × .5 × 4mm length, and bent at 1mm to make an L shaped pin. The pins were then sterilized, and placed in an overnight culture of USA300 LAC::*lux* methicillin resistant *S. aureus*[25] for at least twenty minutes. The inoculation dose was determined to be 200,000 colony forming units by sonicating individual pins and performing serial dilutions on tryptic soy agar plates. Mice were given 60mg/kg ketamine and 4mg/kg xylazine as well as a pre-operative dose of buprenorphine. The right leg was then shaved and washed with 70% ethanol and surgical scrub. A 3–5mm incision was made on the medial aspect of the tibia. The medial tibia was then predrilled using successive 30g and 26g needles before the pin was placed through the defect. The surgical site was closed using 5-0 interrupted sutures. To monitor the infection longitudinally, bioluminescence at the tibia was measured using a Xenogen IVIS camera system (Almeda, CA). BLI is reported as the magnitude of the signal above the noise level (uninfected leg).

Colony Forming Units

S. aureus was isolated and colony forming units quantitated from infected tibia at sacrifice. Necrotic soft tissue surrounding the infection site was first removed. The remaining tissue was disarticulated from the tibia, the pin was removed, and the tibia was placed in 2mL of PBS. Tissues were then homogenized using an IKA T-10 handheld homogenizer (Wilmington, NC). Serial dilutions were then prepared in PBS, and 100uL aliquots were plated on tryptic soy agar. Plates were then placed at 37C for 24 hours before counting colonies.

Micro-computed tomography (μCT)

Tibiae were isolated at the indicated time points and fixed for 3 days in 4% neutral buffered formalin. Specimens were then rinsed in three changes of phosphate buffered saline followed by distilled water. μCT method: Tibiae with infected or sterile pins were harvested 21 and 35 days postoperatively by disarticulating the right lower-extremity at the knee and cutting the tibia just distal to origin of the fibula. High-resolution micro-computed tomography (vivaCT 40; Scanco Medical AG, Basserdorf, Switzerland) was used to render a three-dimensional image of the tibia [26; 27]. Bone volume was accessed using the following parameters: 55 kV energy setting, 300 millisecond integration time, 10.5 μM voxel size, 10 μM slice increment, and a threshold of 210. To analyze reactive bone volume, two contours were created for each slice; the first traced the perimeter of the external reactive bone and the second surrounded all cortical bone from the adjacent uninjured cortices. Subtraction included all mineralized tissues above the threshold between the two contour lines, which encompassed the entire periosteal reaction. Osteolysis was determined from the medial cortex by measuring the total volume of voxels at the pin site.

Histological analysis

Following μCT analysis, samples were decalcified in EDTA for 7 days and then placed in 70% alcohol. Samples were then embedded in paraffin, and 5 micron transverse or sagittal sections were prepared. Safranin O, alcian blue hematoxylin, and tartrate-resistant acid phosphatase staining was performed as previously described [21; 28]. Quantification of histological sections was performed using Osteomeasure (Osteometrics, Decatur GA, USA). *Immunofluorescent staining*: sodium citrate (Dako, Carpinteria CA) was diluted per manufacturers instructions and slides were incubated at 95°C for 40 minutes. Following antigen retrieval, blocking was performed with 10% donkey serum in PBS for 2 hours at RT. Primary antibodies: rabbit anti-osteocalcin (Abcam, Cambridge USA) and anti-F4/80 (Santa Cruz Biotechnology, Dallas USA) at 1:200 in PBS were incubated overnight at 4 °C. Anti-rabbit secondary antibody conjugated to Alexa Fluor 594 (ThermoFisher, Waltham, MA) or mIgGκ BP-CFL 594 (Santa Cruz, Dallas USA) were used at 1:200 for 1 hour in tris-buffered saline, followed by DAPI staining (ThermoFisher), and fixation using ProLong gold antifade mounting reagent (Life Technologies, Eugene, OR). All slides were visualized using an Olympus VS120 virtual slide scanning microscope with Olympus OlyVIA software. *Quantification of osteocalcin*: Osteocalcin staining area was determined using Visiopharm software (Brookfield, CO).

RNA extraction and sequencing

Infected tibia were placed in RNAprotect (Qiagen) immediately after isolation and stored at −80°C. Prior to extraction of RNA, bone was pulverized at liquid nitrogen temperatures. RNA was then extracted by mechanical lysis in ice-cold acid phenol using the Fast-Prep-24 instrument (MP Biomedicals) at a setting of 5.5 for 40s. Extracted RNA was purified using RNeasy mini-columns (Life Technologies). Contaminating genomic DNA was removed using TurboDNase (Ambion). *Illumina library construction for RNAseq:* Libraries were prepared from rRNA-depleted RNA (Ribo-Zero; Epicenter) using the ScriptSeq v2 RNAseq library preparation kit (Epicentre) per the manufacturer's instructions. Libraries were

sequenced on an Illumina HiSeq2500 platform with 4–5 libraries multiplexed per lane and ~50 million 100nt single-direction reads for each sample. Initial sequence data from the HiSeq2500 was evaluated for quality. The low-quality sequence reads were removed prior to final analysis using Seqclean (http://sourceforge.net/projects/seqclean/). The remaining high quality processed reads were then mapped or aligned to the mouse genome (mus musculus) with SHRiMP version 2.2.3 [29] to match sequence reads to specific *mouse* genes. Differential expression levels of all genes were determined using Cufflinks (cuffDiff2) version 2.0.2 [30] and a false discovery rate (FDR) of 0.05, which calculates gene expression as the number of sequence reads that map to each gene. Genes significantly increased or decreased were subjected to pathway analysis using David bioinformatics database [31] and were sorted based on biological process gene ontology terms. Differentially expressed genes between lean and obese/T2D mice at day 14 were also analyzed using BioGPS gene annotation software [32]. Genes with significantly increased or decreased expression were annotated to the cell type most likely to express the enriched gene. At least three mice were used per group for RNAsequencing experiments. All RNA-Seq data (raw sequence reads and primary analysis) were deposited at NCBI and SRA.

Statistics

Multiple analyte comparisons were measured using two-way ANOVA and Bonferroni's post test. Unpaired t-test was used when two groups were compared, including area under the curve measurements. All statistics were analyzed using Graphpad Prism.

RESULTS

Increased MRSA infection in obese/T2D mice

Consistent with our previous studies [13; 15], obese/T2D mice when infected with a USA300 lac::lux MRSA-coated transtibial pin showed an increase in *S. aureus* colony forming units (CFU) in the infected tibia (Obese/T2D: $1.12E^6$ CFU, control: $2.60E^5$ CFU) (Figure 1A). No mortality was observed in either lean or obese mice to day 21. In agreement with the CFU data, an increase in the longitudinal bioluminescence from this strain of *S. aureus* was observed over the 21 day infection in obese/T2D mice compared to controls (Figure 1B, C). The largest difference in bioluminescence was at day 1 post-infection (Figure 1B). No difference in bioluminescent signal was noted at 7 days post-infection. Interestingly, there was a trend towards an increase in obese/T2D mice until sacrifice at day 21. Together, these results demonstrate an increase in *S. aureus* proliferation and survival in obesity/T2D compared to lean-fed control mice.

Gene expression in infected tibiae indicate increased ossification and inflammation in obese/T2D mice following infection

To investigate obese/T2D effects on host responses during *S. aureus* bone infection, we performed whole transcriptome sequencing on RNA from infected tibiae of obese/T2D and control mice harvested on days 7 and 14. Obese/T2D and control mice shared 143 genes that were differentially expressed from day 7 to day 14 (Figure 2A). Pathway analysis demonstrated enrichment for GO terms associated with collagen organization and catabolism, inflammation and immune responses, and bone mineralization (Figure 2B).

There were 635 gene changes from day 7 to day 14 that were unique to obese/T2D mice (Figure 2A). Multiple Gene Ontology terms associated with bone formation were enriched in the obese/T2D mice, including ossification, angiogenesis, osteoblast differentitation, and skeletal system development (Figure 2C, Figure S-1A). Interestingly, multiple terms associated with immune function, including immune response, cellular response to IL-1, defense response to gram positive bacteria, and anti-bacterial humoral response were enriched only in obese/T2D mice. Pathway analysis of the significantly different genes between obese/T2D and control mice at day 14 again demonstrated enrichment for genes associated with immune responses in obesity/T2D (Figure 2D, Figure S-1B). Moreover, anaylsis using Ingenuity Pathway Analysis Software further indicated an enrichment in multiple inflammatory pathways with a positive Z-score (Figure S-1C). Other significantly enriched terms included cell migration in angiogenesis, cytolysis, and fat cell differentiation. Utilizing BioGPS, mast cells, osteoblasts, and macrophages were the cell types most associated with enriched terms in obese/T2D mice. Together, these results indicate altered expression of genes associated with bone formation and immune responses in obese/T2D mice.

Increased periosteal reactive bone formation in obese/T2D following orthopaedic infection

To validate day 14 RNAseq results indicating an obese/T2D-induced bone response during orthopaedic infection, we performed histology and microCT analyses on implanted tibiae both 21 and 35 days post-infection. Histological analysis of the infected tibiae at day 21 revealed new, disorganized bone formation peripheral to the cortical bone in both obese/T2D and co ntrol mice (Figure 3A, B). This new bone formation was consistent with radiographic findings in the osteomyelitis of human patients [3], which indicated robust periosteal reactive bone formation. Quantification of bone volume by microCT revealed twice as much periosteal reactive bone in obese/T2D mice (Figure 3A–C) at 21 and 35 days post-infection. Sterile implants were associated with minimal reactive bone in either group at day 21, indicating that periosteal reactive bone formation is dependent on *S. aureus* infection, and not disruption of the periosteum by an indwelling orthopaedic device (Figure 3A–C). Considerable periosteal reaction was present on both the medial (nearest to pin insertion site) and lateral portion of the tibia at day 21, with more bone evident in both locations in obese/T2D mice (Figure 3A). Similarly, sagittal sectioning at day 35 revealed more periosteal reaction on the anterior surface of the infected tibia of obese/T2D mice (Figure 3A).

In both obese/T2D and control mice, new bone formation extended from the tibial plateau to the insertion of the fibula at day 14 (Figure 3A,4A). This rapid formation of reactive bone was consistent with intramembranous ossification [33]. However, histological sections of infected tibiae at day 14 from obese/T2D mice but not control mice revealed robust numbers of chondrocytes at or near the infection site (Figure 4A, B) and a markedly greater area of proteoglycan rich matrix at the infection site (Figure 4C). Both are indicative of endochondral bone formation. Overall, the majority of periosteal reactive bone does not appear to be endochondreal bone except near the implant site. The latter bone formation is essentially limited to the obese/T2D host. As anticipated, cells associated with new bone stained for osteocalcin, a marker for terminally differentiated chondrocytes and osteoblasts.

Consistent with the formation of more bone in the obese/T2D mice, significantly more osteocalcin staining was observed in the tibia of obese/T2D mice compared to control mice (Figure 4D, E). Moreover, there was a trend towards an increase in osteocalcin area per bone area (Figure 4F). In obese/T2D mice, but not control mice, there was positive osteocalcin staining in both terminally differentiated chondrocytes and osteoblasts (Figure 4D). Hypertrophic chondrocytes, proteoglycan deposition, and osteoblast formation are hallmarks of endochondral ossification. Thus, the increased periosteal reaction in obese/T2D may be due, at least in part, to a different healing process in the bone following infection.

Increased osteolysis in obese/T2D mice

Orthopaedic infection is associated with bone resorption and osteolysis [3; 33]. Expanding on this, RNAsequencing (Figure 2) indicated enrichment for genes associated with regulation of bone resorption in obese/T2D mice. TRAP staining of histologic sections from infected tibiae at day 14 detected osteoclasts along bone surfaces in both obese/T2D and lean mice (Figure 5A) with significantly more in obese/T2D mice (Figure 5B), and more bone surface lined with TRAP+ osteoclasts (Figure 5C). Moreover, there was more TRAP staining per bone surface in either obese/T2D and lean infected mice compared to mice receiving a sterile implant (Figure 5C), indicating that the robust osteoclast activation was a result of *S. aureus* infection, not bone trauma due to insertion of the implant through the cortex of the tibia. The majority of the osteoclasts were found within the reactive bone (Figure 5A, D). Obese/T2D mice had more osteoclast staining within the periosteal reactive bone and along cortical surfaces than lean-fed control mice (Figure 5D). However, the results do not show globally increased osteolysis. Interestingly, there was less osteoclast staining along trabecular surfaces in infected high fat fed-fed mice compared to infected lean-fed mice. One major factor is that obese mice have only 50% of trabecular bone volume of lean mice at the time of infected pin placement[20] (Fig 5E). For unknown reasons, this depleted trabecular bone appears to be markedly less targeted by osteoclasts despite increased osteoclast activity (TRAP staining) in reactive and cortical bone of obese infected mice.

Both obese/T2D and control mice given a sterile implant had very little osteolysis and bone loss around the implant (Figure 5F,H) compared to mice given a *S. aureus*-coated implant (Figure 5F,H). Consistent with increased osteoclast staining (Figure 5D), osteolysis (hole size) was greater in obese/T2D mice (Figure 5F,H). No difference was noted in the volume of sequestrum (dead infected bone) between obese/T2D and control mice (Figure 5G), and no osteoclasts were detected, consistent with this bone being necrotic and inaccessible to host cells. Taken together, obesity/T2D is associated with increased osteoclast activity and osteolytic bone loss following orthopaedic *S. aureus* infection.

Increased macrophage numbers in infected bone in obesity/T2D

Mapping of overexpressed genes in obese/T2D mice to a potential cellular source revealed an enrichment in genes associated with macrophages (Figure 2E). To validate these results we performed immunohistochemistry for F4/80+ macrophages in infected tibiae, which revealed a significant increase in obese/T2D compared to control mice (Figure 6A, B). Macrophages were most prominently located within the marrow space (Figure 6A). However, many macrophages were also noted in the periosteal reactive bone in obese/T2D

mice (Figure 6B). There was a positive correlation between with the number of F4/80+ macrophages in the reactive bone, and the volume of the reactive bone as measure by μCT (Figure 6C).

DISCUSSION

In this study, high fat-fed obese and T2D mice had more periosteal reactive bone, osteolysis, osteoclast activation, and macrophage invasion into the involved bone compared to lean-fed control mice following placement of identical *S. aureus* coated orthopaedic implants. While bone infection is associated with osteolysis and periosteal reaction, whether obesity and diabetes affect these pathological processes had not been determined. It has been shown experimentally that *S. aureus* osteomyelitis is associated with the formation of periosteal reactive bone following *S. aureus* injection into the tibia [18]. Our study demonstrates the formation of robust periosteal reactive bone in the clinically relevant context of an orthopaedic implant pre-coated with USA300 *S. aureus*. We also demonstrate for the first time in an experimental model that obesity/T2D drives a more aggressive periosteal reactive bone formation. The periosteal reaction is dependent on an infection at the implant site, as mice given a sterile implant and simultaneously infected systemically (via a tail vein inoculation) had no reactive bone (data not shown). These studies expand upon our earlier reports which demonstrated more severe implant-associated *S. aureus* infections in our high fat-diet model of obesity/T2D[13]. Taken together, this obesity/T2D mouse model recapitulates the key clinical features of implant-associated orthopaedic infection in these patients[9; 34; 35]. Note that only male C57BL/6 mice were utilized in this study due to the consistency with which they develop a chronic inflammatory state with obesity and glucose intolerance. Female C57BL/6 mice respond more modestly and less consistently to the HF diet with less inflammation, body mass gain and glucose intolerance. This male:female difference in response to HF diet is not seen in human subjects. Based on this more modest obesity/T2D phenotype in female C57BL/6 mice on a HF diet, it is speculated that female C57BL/6 mice would have a less severe infection, but this will require further investigation.

Recent reports indicate that bacterial virulence genes expressed at the site of infection are the primary triggers for bone remodeling in osteomyelitis [18; 19]. Our previous study demonstrated a 5-fold (although not statistically significant) increase in *sarA* expression in *S. aureus* isolated from obese/T2D infected mice compared to *S. aureus* isolated from control mice[15]. SarA has been shown to be an important virulence factor driving bone destruction in osteomyelitis [19], raising the possibility that the increased osteolysis in obese/T2D mice may be driven by *S. aureus* gene expression changes representing adaptation to the unique environment of the obese/T2D host. Our additional reporting of markedly upregulated gene expression of *S. aureus* matrix-binding proteins in bacteria isolated from infected bone of obese/T2D mice further supports this premise of adaptation.

Our findings confirm previous studies demonstrating *S. aureus* causes significant bone destruction in osteomyelitis. Both obese/T2D and control mice had significant cortical bone loss at the implant site compared to mice administered a sterile pin. Furthermore, osteolysis in cortical bone of obese mice, as assessed by μCT, was greater at day 21 than in lean controls. This more robust osteolysis in infected cortical bone of obese mice was further

supported by increased TRAP+ osteoclast staining at day 14. In contrast to cortical bone that showed both increased osteolysis and increased TRAP staining, the strong positive TRAP staining in periosteal bone of obese mice was associated with increased formation. In light the large periosteal reactive bone formation, both robust bone formation and osteoclast-mediated resorption appear to be occurring with the balance in favor of bone formation. Trabecular bone of infected lean mice showed positive TRAP staining that was associated with a 50% loss of bone volume (Fig 5E). Surprisingly, trabecular bone of obese infected mice showed minimal TRAP staining and no loss of bone volume. High fat diet-fed obese mice, however, have only 50% of the trabecular bone of lean mice (Fig. 5E and ref. 20). This depleted trabecular bone appears to be resistant to targeting by osteoclasts during infection.

There is a temporal and spatial association between periosteal reactive bone formation, TRAP+ staining, and macrophage presence. This suggests that the increased osteoclastogenesis is driven by factors related to an increased inflammatory environment in the infected bone of the obese/T2D host. For example, TNF, a common inflammatory mediator in infection and a cytokine that is elevated in obesity/T2D, is well known to enhance osteoclastogenesis [36]. Similarly, inflammation has been suggested to be a contributor to reactive bone formation [37]. Future investigations with this mouse implant infection model in the context of obesity/T2D will be designed to address these relationships. In general, the increased bone loss in an infected orthopaedic implant in obesity/T2D such as modeled here would increase the risk for implant loosening and failure, and reduce available bone surface for any subsequent revision surgery [3].

The disorganization and the rate at which periosteal reactive bone appeared was consistent with intramembranous bone formation in both control and obese/T2D mice [33]. In general, the histologic results supported this conclusion. However, there was evidence of endochondral bone formation in obese/T2D mice proximal to the implant insertion site but not in control mice (Figure 2, 3). Consistent with endochondral bone formation [33], there were markedly more chondrocytes and substantially more proteoglycan deposition in infected bone from obese/T2D mice. The proteoglycan-rich matrix was most evident at the periosteum nearest the site of the infection. While the stimulus for this endochondral bone formation is unclear at this time, it is intriguing that it occurs essentially only in obese/T2D mice that have a more severe osteomyelitis. RNAsequencing indicated an enrichment in GO terms in the infected bone of obese/T2D mice that are associated with ossification, osteoblast differentiation, angiogenesis, and skeletal system development. This was certainly consistent with the more abundant reactive bone of obese/T2D mice as well as the endochondral ossification. Increased osteocalcin staining in the infected bone of obese/T2D mice demonstrated more abundant osteoblasts and further supported the RNA sequencing data. Taken together, the RNA sequencing data coupled with histologic and microCT imaging data demonstrate that a more severe periosteal reactive bone formation occurs in the *S. aureus* bone infections of obesity and type 2 diabetes.

Together, the current data indicate an increase in both pathological bone loss and new periosteal reactive bone formation in obese/T2D mice. As revealed by the RNA sequencing data and pathway analysis, these two pathologic bone processes coincided with increased immune cell recruitment and inflammation in bone of obese/T2D mice. Multiple GO terms

associated with inflammatory responses, such as antibacterial humoral response, immune response, cellular response to IL-1, and defense response to gram-positive bacteria were all enriched in obese/T2D mice from day 7 to day 14 following infection. Additionally, when aligned with the mRNA reference bank BioGPS, several upregulated genes associated with macrophages and mast cells were elevated in bone of obese/T2D mice. These data were corroborated by our immunohistochemical evidence of more abundant F4/80+ macrophages within and lining the periosteal reactive bone in obese/T2D mice (Figure 5). It is also tempting to link in a cause and effect relationship the increase in pro-inflammatory cells recruited to the infected bone of obese/T2D mice to the increases in both the osteolysis and periosteal bone formation. Additionally, the pro-inflammatory cells may at least in part be more abundant because of the increase in *S. aureus* load in obesity/T2D. Further investigations are required to establish the relationships between the critical events in this pathologic process. Nonetheless, proposing causal linkage between the above events is not without support. Several labs have reported that IL1-β, an inflammatory cytokine produced primarily by macrophages, is sufficient to induce differentiation of human MSCs to osteoblasts [38; 39]. IL-6, a pro-inflammatory cytokine produced by macrophages that is known to be elevated in high fat-fed mice [22], has been shown to positively regulate chondrogenic differentiation of MSCs [40]. Moreover, multiple pro-inflammatory cytokines such as TNF [36] and IL-6 [41] have been shown to be involved in osteoclast activation. Therefore, we speculate that the increased inflammatory state in the infected bone of obese/T2D mice is the primary driver of both the increased periosteal reactive bone and bone destruction in obese, type 2 diabetic hosts. Future studies will be conducted to further test this hypothesis.

In conclusion, it is demonstrated here that implant-associated *S. aureus* infection and accompanying bone responses of periosteal reactive bone formation and osteolytic bone destruction are more severe in the obese/T2D host. Controlling these pathologic processes may be a therapeutic strategy in treating the complications of osteomyelitis in the obese/T2D population.

Supplementary Material

Refer to Web version on PubMed Central for supplementary material.

Acknowledgments

The authors wish to thank Ann Gill, Sarah Mack, Kathy Maltby, and Mike Thullen for their very capable technical skills. The support of the Histology, Biochemistry, and Molecular Imaging Core in the Center for Musculoskeletal Research at the University of Rochester is greatly appreciated. RNA-Seq and transcriptome analysis described in this study was completed by the University of Rochester Genomics Research Center (URGRC). This work was supported by AOTrauma Research (CPP Bone Infection), NIH P30 AR069655, NIH P50 AR 072000, and NIH T32 AR053459.

References

1. Kurtz SM, Lau E, Schmier J, et al. Infection burden for hip and knee arthroplasty in the United States. The Journal of arthroplasty. 2008; 23:984–991. [PubMed: 18534466]
2. Cram P, Lu X, Kates SL, et al. Total knee arthroplasty volume, utilization, and outcomes among Medicare beneficiaries, 1991–2010. Jama. 2012; 308:1227–1236. [PubMed: 23011713]

3. Lew DP, Waldvogel FA. Osteomyelitis. Lancet. 2004; 364:369–379. [PubMed: 15276398]
4. Kamath AF, Ong KL, Lau E, et al. Quantifying the Burden of Revision Total Joint Arthroplasty for Periprosthetic Infection. The Journal of arthroplasty. 2015; 30:1492–1497. [PubMed: 25865815]
5. Nishitani K, Sutipornpalangkul W, de Mesy Bentley KL, et al. Quantifying the natural history of biofilm formation in vivo during the establishment of chronic implant-associated Staphylococcus aureus osteomyelitis in mice to identify critical pathogen and host factors. Journal of orthopaedic research : official publication of the Orthopaedic Research Society. 2015; 33:1311–1319. [PubMed: 25820925]
6. Birt MC, Anderson DW, Bruce Toby E, et al. Osteomyelitis: Recent advances in pathophysiology and therapeutic strategies. Journal of orthopaedics. 2017; 14:45–52. [PubMed: 27822001]
7. Kini SG, Gabr A, Das R, et al. Two-stage Revision for Periprosthetic Hip and Knee Joint Infections. The open orthopaedics journal. 2016; 10:579–588. [PubMed: 28144371]
8. Dowsey MM, Choong PF. Obese diabetic patients are at substantial risk for deep infection after primary TKA. Clinical orthopaedics and related research. 2009; 467:1577–1581. [PubMed: 18841430]
9. Jamsen E, Nevalainen P, Eskelinen A, et al. Obesity, diabetes, and preoperative hyperglycemia as predictors of periprosthetic joint infection: a single-center analysis of 7181 primary hip and knee replacements for osteoarthritis. The Journal of bone and joint surgery American volume. 2012; 94:e101. [PubMed: 22810408]
10. Wu C, Qu X, Liu F, et al. Risk factors for periprosthetic joint infection after total hip arthroplasty and total knee arthroplasty in Chinese patients. PloS one. 2014; 9:e95300. [PubMed: 24748009]
11. Strandberg L, Verdrengh M, Enge M, et al. Mice chronically fed high-fat diet have increased mortality and disturbed immune response in sepsis. PloS one. 2009; 4:e7605. [PubMed: 19865485]
12. Amar S, Zhou Q, Shaik-Dasthagirisaheb Y, et al. Diet-induced obesity in mice causes changes in immune responses and bone loss manifested by bacterial challenge. Proceedings of the National Academy of Sciences of the United States of America. 2007; 104:20466–20471. [PubMed: 18077329]
13. Farnsworth CW, Shehatou CT, Maynard R, et al. A humoral immune defect distinguishes the response to Staphylococcus aureus infections in mice with obesity and type 2 diabetes from that in mice with type 1 diabetes. Infection and immunity. 2015; 83:2264–2274. [PubMed: 25802056]
14. Milner JJ, Sheridan PA, Karlsson EA, et al. Diet-induced obese mice exhibit altered heterologous immunity during a secondary 2009 pandemic H1N1 infection. Journal of immunology (Baltimore, Md : 1950). 2013; 191:2474–2485.
15. Farnsworth CW, Schott EM, Jensen SE, et al. Adaptive Upregulation of Clumping Factor A (ClfA) by Staphylococcus aureus in the Obese, Type 2 Diabetic Host Mediates Increased Virulence. Infection and immunity. 2017; 85:e01005–01016. [PubMed: 28320836]
16. de Mesy Bentley KL, Trombetta R, Nishitani K, et al. Evidence of Staphylococcus Aureus Deformation, Proliferation, and Migration in Canaliculi of Live Cortical Bone in Murine Models of Osteomyelitis. Journal of bone and mineral research : the official journal of the American Society for Bone and Mineral Research. 2016
17. Wright JA, Nair SP. Interaction of staphylococci with bone. International journal of medical microbiology : IJMM. 2010; 300:193–204. [PubMed: 19889575]
18. Cassat JE, Hammer ND, Campbell JP, et al. A secreted bacterial protease tailors the Staphylococcus aureus virulence repertoire to modulate bone remodeling during osteomyelitis. Cell host & microbe. 2013; 13:759–772. [PubMed: 23768499]
19. Loughran AJ, Gaddy D, Beenken KE, et al. Impact of sarA and Phenol-Soluble Modulins on the Pathogenesis of Osteomyelitis in Diverse Clinical Isolates of Staphylococcus aureus. Infection and immunity. 2016; 84:2586–2594. [PubMed: 27354444]
20. Inzana JA, Kung M, Shu L, et al. Immature mice are more susceptible to the detrimental effects of high fat diet on cancellous bone in the distal femur. Bone. 2013; 57:174–183. [PubMed: 23954757]

21. Brown ML, Yukata K, Farnsworth CW, et al. Delayed fracture healing and increased callus adiposity in a C57BL/6J murine model of obesity-associated type 2 diabetes mellitus. PloS one. 2014; 9:e99656. [PubMed: 24911161]
22. Gregor MF, Hotamisligil GS. Inflammatory mechanisms in obesity. Annu Rev Immunol. 2011; 29:415–445. [PubMed: 21219177]
23. Xu H, Barnes GT, Yang Q, et al. Chronic inflammation in fat plays a crucial role in the development of obesity-related insulin resistance. The Journal of clinical investigation. 2003; 112:1821–1830. [PubMed: 14679177]
24. Beier EE, Inzana JA, Sheu TJ, et al. Effects of Combined Exposure to Lead and High-Fat Diet on Bone Quality in Juvenile Male Mice. Environ Health Perspect. 2015; 123:935–943. [PubMed: 25861094]
25. Thurlow LR, Hanke ML, Fritz T, et al. Staphylococcus aureus biofilms prevent macrophage phagocytosis and attenuate inflammation in vivo. Journal of immunology (Baltimore, Md : 1950). 2011; 186:6585–6596.
26. Kung MH, Yukata K, O'Keefe RJ, et al. Aryl hydrocarbon receptor-mediated impairment of chondrogenesis and fracture healing by cigarette smoke and benzo(a)pyrene. Journal of cellular physiology. 2012; 227:1062–1070. [PubMed: 21567390]
27. Dhillon RS, Schwarz EM. Teriparatide Therapy as an Adjuvant for Tissue Engineering and Integration of Biomaterials. Journal of materials research. 2011; 4:1117–1131. [PubMed: 21857768]
28. Mooney RA, Sampson ER, Lerea J, et al. High-fat diet accelerates progression of osteoarthritis after meniscal/ligamentous injury. Arthritis research & therapy. 2011; 13:R198. [PubMed: 22152451]
29. David M, Dzamba M, Lister D, et al. SHRiMP2: sensitive yet practical SHort Read Mapping. Bioinformatics. 2011; 27:1011–1012. [PubMed: 21278192]
30. Trapnell C, Roberts A, Goff L, et al. Differential gene and transcript expression analysis of RNA-seq experiments with TopHat and Cufflinks. Nature protocols. 2012; 7:562–578. [PubMed: 22383036]
31. Huang da W, Sherman BT, Lempicki RA. Systematic and integrative analysis of large gene lists using DAVID bioinformatics resources. Nature protocols. 2009; 4:44–57. [PubMed: 19131956]
32. Wu C, Orozco C, Boyer J, et al. BioGPS: an extensible and customizable portal for querying and organizing gene annotation resources. Genome biology. 2009; 10:R130. [PubMed: 19919682]
33. O'Keefe, RJJJ., Chu, CR., Einhorn, TA. Orthopaedic Basic Science: Foundations of Clinical Practice. 4. Rosemont, IL: American Academy of Orthopaedic Surgeons;; 2013.
34. Winfield RD, Reese S, Bochicchio K, et al. Obesity and the Risk for Surgical Site Infection in Abdominal Surgery. The American surgeon. 2016; 82:331–336. [PubMed: 27097626]
35. Huttunen R, Syrjanen J. Obesity and the risk and outcome of infection. International journal of obesity (2005). 2013; 37:333–340. [PubMed: 22546772]
36. Boyce BF, Li P, Yao Z, et al. TNF-alpha and pathologic bone resorption. The Keio journal of medicine. 2005; 54:127–131. [PubMed: 16237274]
37. Raymond AK, Jaffe N. Conditions that mimic osteosarcoma. Cancer Treat Res. 2009; 152:85–121. [PubMed: 20213387]
38. Sonomoto K, Yamaoka K, Oshita K, et al. Interleukin-1beta induces differentiation of human mesenchymal stem cells into osteoblasts via the Wnt-5a/receptor tyrosine kinase-like orphan receptor 2 pathway. Arthritis and rheumatism. 2012; 64:3355–3363. [PubMed: 22674197]
39. Ferreira E, Porter RM, Wehling N, et al. Inflammatory cytokines induce a unique mineralizing phenotype in mesenchymal stem cells derived from human bone marrow. The Journal of biological chemistry. 2013; 288:29494–29505. [PubMed: 23970554]
40. Kondo M, Yamaoka K, Sakata K, et al. Contribution of the Interleukin-6/STAT-3 Signaling Pathway to Chondrogenic Differentiation of Human Mesenchymal Stem Cells. Arthritis & rheumatology (Hoboken, NJ). 2015; 67:1250–1260.
41. Gao Y, Morita I, Maruo N, et al. Expression of IL-6 receptor and GP130 in mouse bone marrow cells during osteoclast differentiation. Bone. 1998; 22:487–493. [PubMed: 9600782]

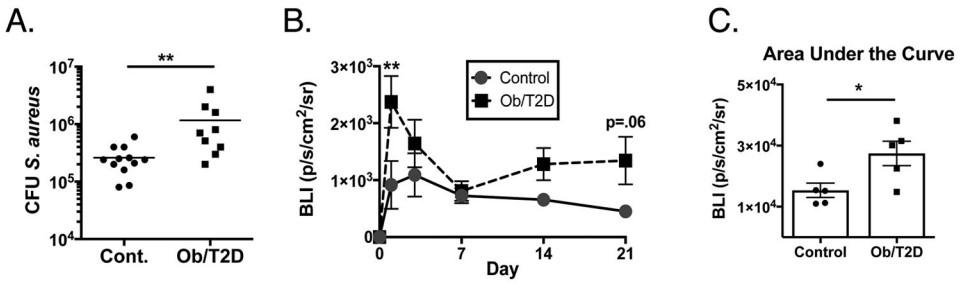

Figure 1. Increased S. aureus proliferation in obese/T2D mice following orthopaedic infection

Mice were fed a high fat-diet to induce obesity/T2D or a control diet for 3 months. Mice were then infected with a trans-tibial pin pre-coated with *S. aureus* USA300 lac::lux. **A.** At 21 days post infection, tibia were harvested and *S. aureus* CFUs were quantitated. n ≥ 9. **B.** Time course of bioluminescent signal emitted at the implant site from luminescent *S. aureus* containing the *lux a-e* operon indicating *S. aureus* proliferation. n = 5. **C.** Area under the curve for **B.** * P<.05, ** p<.01. Unpaired student T test for A and C. Two way Anova was used for B with Tukey post-hoc test. In A, C, each point represents one mouse.

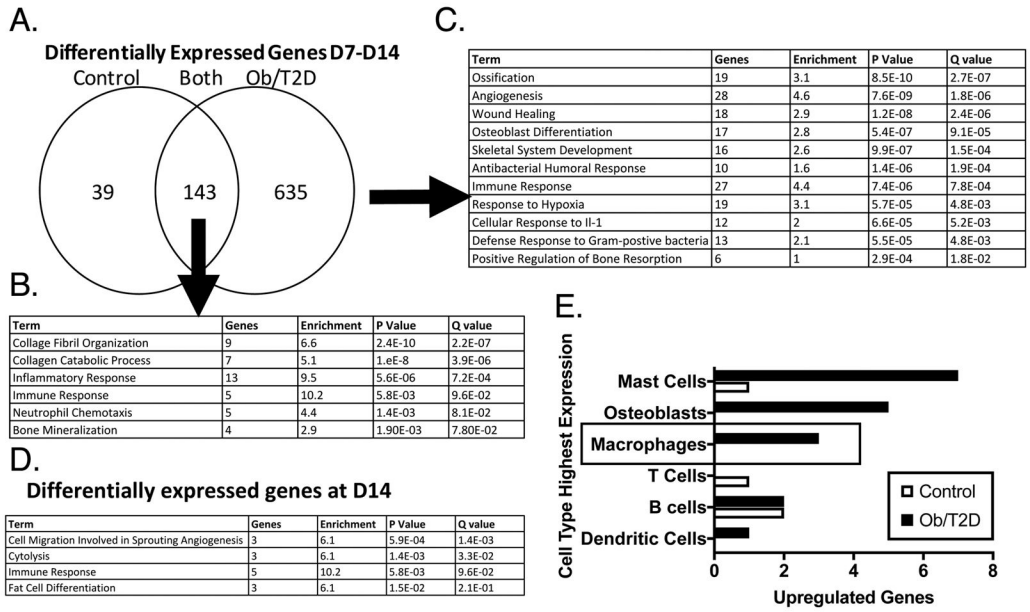

Term	Genes	Enrichment	P Value	Q value
Collage Fibril Organization	9	6.6	2.4E-10	2.2E-07
Collagen Catabolic Process	7	5.1	1.eE-8	3.9E-06
Inflammatory Response	13	9.5	5.6E-06	7.2E-04
Immune Response	5	10.2	5.8E-03	9.6E-02
Neutrophil Chemotaxis	5	4.4	1.4E-03	8.1E-02
Bone Mineralization	4	2.9	1.90E-03	7.80E-02

Term	Genes	Enrichment	P Value	Q value
Ossification	19	3.1	8.5E-10	2.7E-07
Angiogenesis	28	4.6	7.6E-09	1.8E-06
Wound Healing	18	2.9	1.2E-08	2.4E-06
Osteoblast Differentiation	17	2.8	5.4E-07	9.1E-05
Skeletal System Development	16	2.6	9.9E-07	1.5E-04
Antibacterial Humoral Response	10	1.6	1.4E-06	1.9E-04
Immune Response	27	4.4	7.4E-06	7.8E-04
Response to Hypoxia	19	3.1	5.7E-05	4.8E-03
Cellular Response to Il-1	12	2	6.6E-05	5.2E-03
Defense Response to Gram-postive bacteria	13	2.1	5.5E-05	4.8E-03
Positive Regulation of Bone Resorption	6	1	2.9E-04	1.8E-02

Term	Genes	Enrichment	P Value	Q value
Cell Migration Involved in Sprouting Angiogenesis	3	6.1	5.9E-04	1.4E-03
Cytolysis	3	6.1	1.4E-03	3.3E-02
Immune Response	5	10.2	5.8E-03	9.6E-02
Fat Cell Differentiation	3	6.1	1.5E-02	2.1E-01

Figure 2. RNA sequencing and pathway analysis in infected bone indicate enrichment in terms associated with inflammation and ossification in obese/T2D mice

Obese/T2D mice and control mice were infected as before and harvested at days 7 and 14 post-infection. Infected tibiae were isolated, homogenized, RNA isolated, and RNAsequencing was performed. **A.** The number of changed genes from day 7 to day 14 in control mice only, obese/T2D mice only, and control and obese/T2D. **B.** Enriched pathways represented by the 143 genes differentially expressed in both obese/T2D and control mice. **C.** Enriched pathways represented by the 635 genes differentially expressed in obese/T2D mice. **D.** Pathways represented by differentially expressed genes between obese/T2D and control mice at day 14. **E.** The 25 genes with the greatest change were mapped to the cell type most likely to express the gene using BioGPS. Genes associated with macrophages and osteoblasts were more highly enriched in obese/T2D mice compared to control mice. n = 3 mice per group.

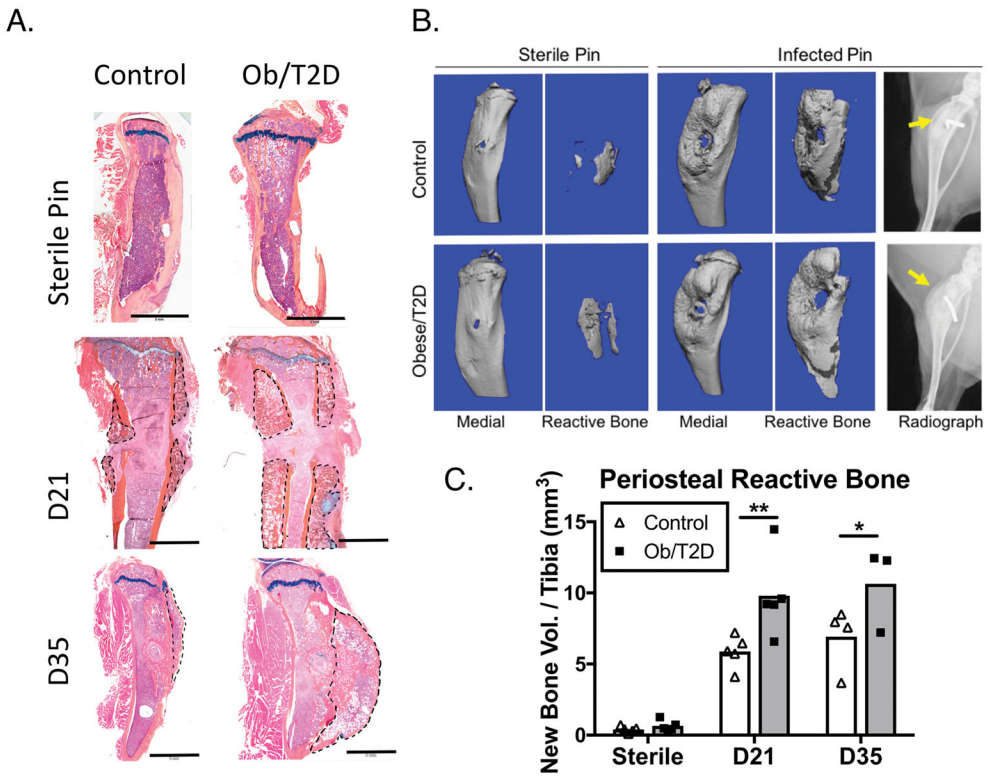

Figure 3. Increased periosteal reactive bone following implant associated *S. aureus* infection in obesity/T2D

Mice received trans-tibial implants as in Figure 1, and tibiae were harvested at days 21 and 35 after infection. **A.** Saggital sections of sterile and infected tibiae at day 21 and coronal sections of infected tibiae at day 35 were stained with Alcian blue orange G hematoxylin. Periosteal reactive bone is outlined in black dashed lines. **B.** Radiographs and μCT reconstructions of affected tibiae with new bone formation distinguished using density thresholding. **C.** Quantitation of new bone from **B.** Scale bars in **A.** are 2mm. *p<.05, ** p <.01. #p<.001 vs infected mice (D21 or D35). Two way ANOVA and Tukey's post-hoc test. N = 3–5 with each point representing one mouse.

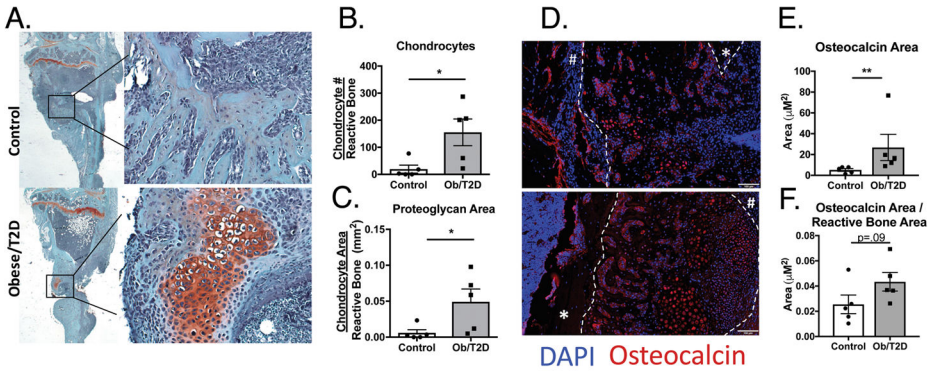

Figure 4. Increased chondrocytes and osteoblasts proximal to the infected implant site in obese/T2D mice

Infected tibiae from obese/T2D and control mice were harvested at day 14. **A.** Sections stained with safranin O revealed proteoglycan-rich areas near the infection site only in obese/T2D mice. Osteomeasure software was utilized to quantify **B.** hypertrophic chondrocytes and **C.** proteoglycan area. **D.** Infected tibiae were stained for osteocalcin (Red) and counterstained with DAPI to visualize osteoblasts and terminally differentiated chondrocytes. Visiopharm software was used to quantify **E.** total osteocalcin area and **F.** osteocalcin area/reactive bone area. * p<.05, **p<.01. Unpaired Student T-test used for B,C,F. Mann Whitney u test used for E. White dashed lines outline the periosteal reactive bone. # identifies the distal edge of the periosteum and * identifies cortical bone. In B, C, E, and F, n = 5 mice per group with each point representing one mouse.

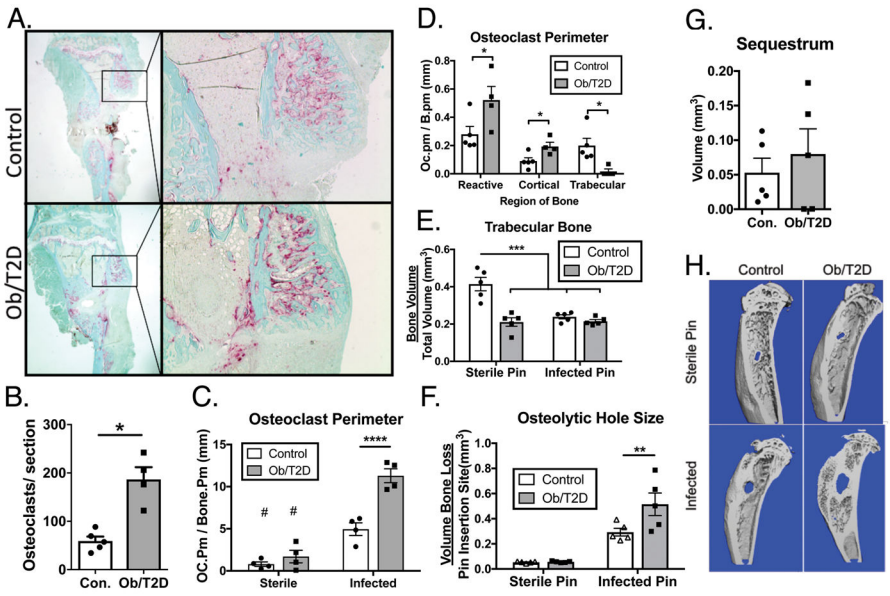

Figure 5. Increased osteoclast activity and osteolysis in infected tibiae of obese/T2D mice

Infected tibiae from obese/T2D and control mice were harvested at day 21. **A.** tartrate-resistant acid phosphatase staining of histologic sections. **B.** the number of osteoclasts per section was quantified. **C.** Osteomeasure software was used to quantitate total perimeter of osteoclast (Trap+), and **D.** Trap+ staining in each bone compartment. μCT was used at day 21 to quantify **E.** total trabecular bone, **F.** osteolytic hole size at the pin insertion site, and **G.** sequestrum (infected necrotic bone). **H.** Representative μCT scans at day 21 post-infection. * p <.05, ** p<.01, *** p <.001. # p <.001 when compared to infected counterpart. #p<.001, $ p<.0001 when comparing non-infected control to infected. Unpaired T-test was used for **B**, **D**, **and H.** Two way ANOVA was used for **C**, **E**, and **G** with Bonferoni correction. n = 4 – 5 mice per group. Each point represents one mouse.

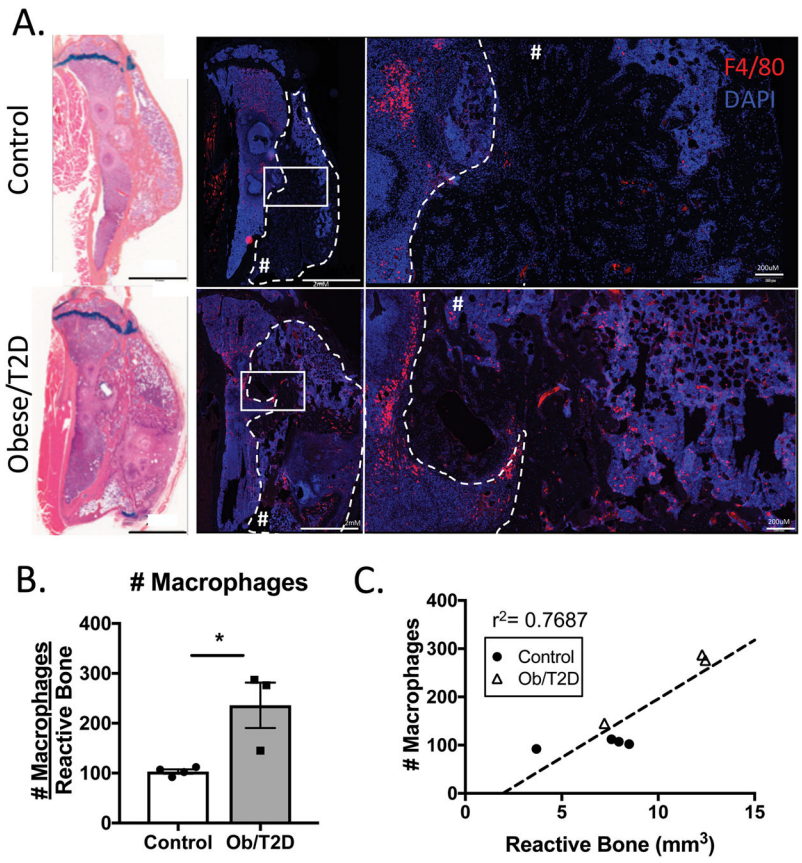

Figure 6. Increased F4/80+ macrophages in infected tibiae of obese/T2D mice

Mice were harvested at day 35 post placement of infected implant. Histological sections were immunostained for F4/80 to visualize macrophages. **A.** Representative images demonstrating increased macrophages in the marrow space and periosteal reactive bone of obese/T2D mice. Paired Alcian blue hematoxylin stained sections reveal the region of interest. Periosteal reactive bone is outlined with dashed lines and denoted with #. **B.** Quantitation of F4/80+ cells in the ROI (Inside dashed lines in **A.**). C. Linear regression analysis demonstrating the correlation between number of macrophages within the periosteal reactive bone ROI and the volume of reactive bone within the ROI. Scale bar length is 2mm. * $p<.05$ unpaired t test. $n \geq 3$. Each point represents one mouse.